ISABE-2015-20241

Fatigue crack propagation study of a Ni-base jet engine material

Youri N Lenets

Alonso Peralta

James Neumann

Ross Miller

Honeywell Aerospace, Phoenix, Arizona, USA

ABSTRACT

The majority of fatigue crack growth tests worldwide makes use of the compact tension (CT) specimens that are not necessarily representative of cracks developing under service conditions in highly stressed components of a jet engine. Over the years other geometries have been designed to facilitate a study of relatively small, semi- or quarter-elliptical surface flaws subjected to high tensile and compressive stresses. Despite an extensive use by the aerospace community, practical aspects of testing and data analysis relevant to the complex surface- or corner-flawed geometries are not regulated by a commonly accepted set of rules.

Two types of test specimens – CT and surface-crack tension (SCT) – were machined from a forged and heat treated Inconel 718. For both geometries the crack orientation and propagation direction with respect to the original forging were the same. At high ΔK values both geometries produced similar results, however, as the ΔK values decreased, a trend towards slower crack growth rates in the SCT specimens became evident.

The CT specimens were tested in accordance with the ASTM Standard E647 as well as using an alternative compression pre-cracking procedure. After correct application of the compression pre-cracking both approaches had yielded reasonably consistent results.

In order to address a so-called small-crack effect, several SCT specimens received much smaller crack starter notches produced by the focused ion beam (FIB) technology.

The results of the present study highlight the importance of the appropriate material properties for accurate and reliable service life prediction of the critical aerospace propulsion hardware with particular emphasis on the influence of specimen/crack geometry and test method on the fatigue crack propagation behavior of jet engine alloys.

NOMENCLATURE

ASTM	American Society for Testing of Materials
a	depth of a crack
c	half surface length of a crack
c/a	crack aspect ratio
da/dN	crack growth rate in depth direction
CT	compact test specimen, loaded in tension
DCEPD	direct current electric potential drop
EDM	electro-discharge machining
EPD	electric potential drop
ESR	electroslag re-melting
FAA	Federal Aviation Administration
FCG	fatigue crack growth
FIB	focused ion beam
GTE	gas turbine engine
LEFM	linear-elastic fracture mechanics
LSG	low stress grind machining
N	number of load cycles
SCT	surface crack test specimen, loaded in tension
SEM	scanning electron microscope
VIM	vacuum-induction melting
VAR	vacuum arc re-melting
ΔK	stress intensity factor range

INTRODUCTION

Gas turbine engine components are subjected in service to a complex interaction between fluctuating stresses and temperatures with operational limits that have a propensity to creep up in a never-ending quest for more thrust, better fuel economy and cost-effective overall design. Due to superb

combination of high-temperature mechanical properties, nickel-base superalloys have long ago become the material of choice for use in the hot section of a jet engine. Recently introduced new requirements for engine manufacturers to conduct a damage tolerance assessment of all rotating structural parts necessitated a thorough understanding of crack behavior in the superalloys under representative service conditions.

The majority of fatigue crack growth (FCG) tests worldwide makes use of the CT specimens containing through-the-thickness defects that are not necessarily representative of cracks developing under service conditions in highly stressed components of a jet engine. In the latter case, due to the frequently present highest stress and temperatures at the outer boundary and to the increased probability of defects, surface cracks are a common occurrence. Therefore, other geometries were designed to facilitate a study of relatively small, semi- or quarter-elliptically shaped surface flaws subjected to high tensile and compressive stresses. Despite an extensive use by the aerospace community, practical aspects of testing and data analysis relevant to the non-trivial surface- or corner-flawed geometries are not regulated by a commonly accepted set of rules (e.g., ASTM Standard E647). Some idiosyncrasies associated with testing and data analysis of two-dimensional cracks in the surface crack tension specimens were previously discussed in [1], while a further comparison of the FCG behavior in the CT and SCT geometries is presented and discussed in following sections of this paper.

Historically, tensile cyclic loading per an assortment of load-shedding schedules had been commonly employed to create and "condition" a crack in the notched laboratory specimens of metallic materials, whereas compressive cyclic loading was regarded as the preferred and, sometimes, the only way to safely pre-crack notched samples of extremely brittle materials (e.g., ceramics). In recent decades, the latter approach has seen renewed interest as a possible alternative for generating higher fidelity FCG data (particularly in near-threshold regime) with minimal load history effects [2-4]. The underlying physical processes of the Mode I FCG in notched specimens of metallic alloys repeatedly subjected to fully compressive cyclic loads, the genesis and practical advantages of the compression pre-cracking methodology as well as some exploratory results regarding the application of the technique to the SCT geometry are available from elsewhere [1].

CT specimens and SCT specimens with electro-discharge machined (EDM) semi-circular crack starter notch of about 0.01" (0.25 mm) radius were tested in accordance with the ASTM Standard E647 as well as using an alternative compression pre-cracking procedure. After correct application of the compression pre-cracking to the CT geometry both approaches had yielded reasonably consistent results. At high ΔK values both studied geometries also produced similar results, however, as the ΔK values decreased, a trend towards slower crack growth rates in the SCT specimens became evident.

Finally, in order to address a so-called small-crack effect, several SCT specimens received much smaller crack starter notches (0.0001" to 0.0002" or 0.025 mm to 0.05 mm) produced by the focused ion beam (FIB) technology. Small, but nonetheless significant difference, consistent with the micro-structural condition of the tested material, was noted between the cracks propagating in the SCT specimens from the smaller FIB notches and much larger cracks propagating from typically used 0.02" (0.5 mm) long EDM notches.

MATERIAL

The material tested in the current study was a conventionally forged precipitation-hardenable Ni-Cr-alloy Inconel 718, containing significant amounts of Fe, Nb, and Mo along with lesser amounts of Al and Ti, produced and heat treated in accordance with the specification for turbine disc applications. A so-called Delta-conversion Process (DP) was specifically developed to eliminate occasional large grains in otherwise fine grain material that are known to contribute to the inferior low cycle fatigue (LCF) life by becoming premature crack initiation sites. The grain size and room temperature tensile properties of the material are summarized in Table 1.

Table 1. Summary of tested material

Designation	ASTM grain size/ Grain diameter, µm	RT YS, ksi/MPa	RT UTS, ksi/MPa
DP718	10-12/11-6	174/1200	205/1413

The DP718 billet was made from a triple melt ingot through vacuum-induction melting (VIM) followed by electroslag re-melting (ESR), and finished by vacuum arc re-melting (VAR). The DP718 material derives its LCF and tensile strength benefits from a consistently fine microstructure resulting from a delta-processing treatment of the raw material when it is being manufactured into billet. The processing occurs during initial ingot breakdown when a special delta-phase precipitation heat treatment is added to the customary billet manufacture. This heat treatment essentially consists of a long soak for 24 hours at approximately 1650F. The delta-phase consists of Ni_3Nb precipitates, which act to inhibit grain growth from any potential re-crystallization operations during final billet working. After the delta-phase heat treatment, final billet working is performed at temperatures less than the delta-solvus to ensure fine

microstructure.

Forging temperatures are generally well below typical delta-solvus temperatures of 1850F to 1875F, which also ensure that the fine microstructure is maintained.

After forging, the final heat treatment of DP718 consisted of a solution treatment below delta-solvus followed by two-step aging process. The solution temperature is typically near the delta-solvus to avoid grain growth. Since delta-solvus is in the range of 1850F to 1875F, the solution temperatures often range from 1800F to 1850F to maintain a fine microstructure while achieving the best delta precipitation possible. The first and second age cycles result in precipitates which are the primary strengthening phases, gamma double-prime with some contribution from the gamma prime phase. The resulting microstructure is shown in Figure 1.

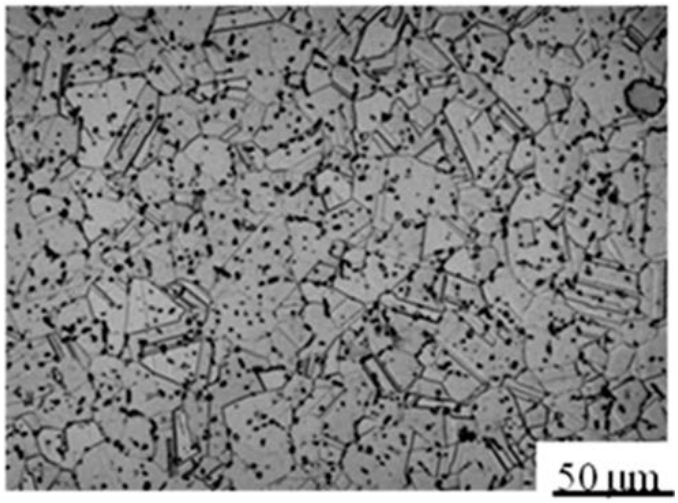

Figure 1. DP 718 microstructure

TEST SPECIMENS PREPARATION

All specimens tested in this study were machined out of the same forging that was used in the previous investigation [1]. The SCT and CT specimens were excised from a central location of the forging and, therefore, the gauge sections of both had a similar microstructure. The crack orientation and propagation direction were also similar as shown schematically in Figure 2.

To eliminate a possibility of fatigue cracks originating from pinholes during pre-cracking, several CT specimens were pre-cracked in compression between two parallel plates prior to pinholes machining. After pre-cracking, the pinholes were machined and their internal surfaces were polished to prevent cracking during the tension test.

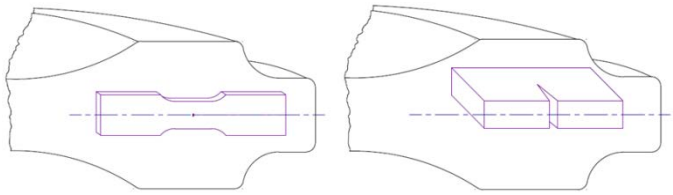

Figure 2. Orientation of the test specimens with respect to forging

The near-surface residual stresses remaining after a low stress grind (LSG) machining of the SCT specimens designated to receive FIB notches were deemed unacceptably high for the purpose of the study. Therefore, a multi-step polishing procedure, developed at Honeywell, was applied to remove at least 0.0005" (0.0127 mm) and to reduce the surface residual stress to acceptable level. In addition, for both geometries studied the material along the anticipated crack trajectory on specimen faces was mechanically polished to facilitate an optical observation and measurement.

In several previously published studies, including [1], FIB notches had a rectangular shape illustrated by Figure 3a. While being easy to produce, such shape also creates a crack driving force substantially different from that calculated for an identically loaded semi-elliptical defect of the same surface length and depth (Figure 3c).

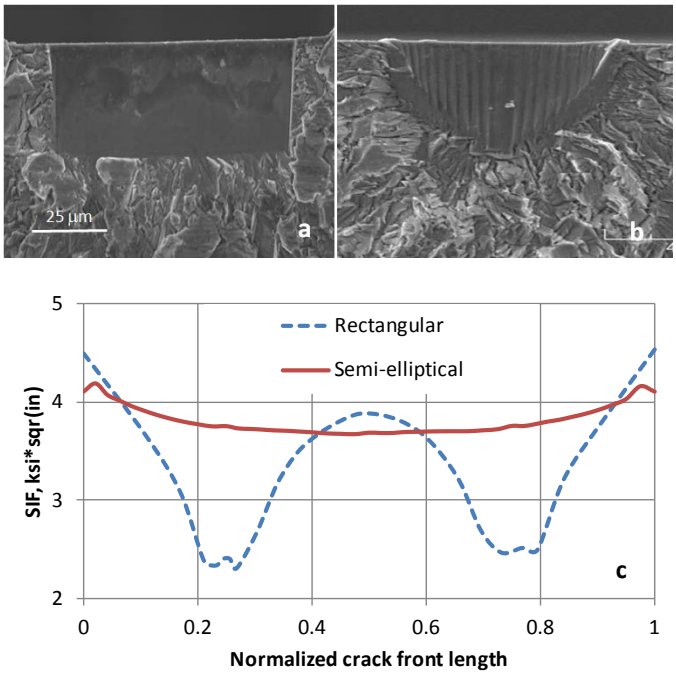

Figure 3. FIB notches of different shape (a, b) and corresponding stress intensities (c)

As a result, an initial propagation stage of cracks emanating from a rectangular FIB notch is influenced not only by the crack dimensions, but also by the originally "unnatural"

crack shape. The latter may have undesired confounding effect on the crack propagation behavior and would definitely require additional non-trivial analytical efforts in order to be accurately deducted from the test outcome. Therefore, in the current study a conscious effort was made to optimize the shape of FIB notches as shown in Figure 3b.

Another improvement in specimen preparation was associated with a FIB notch pattern. In the previous study, all FIB notches were placed along the gauge section on one side of an SCT specimen (an example schematic is available in [1]). Such a pattern has two shortcomings that became evident after initial tests: it requires (i) constant temperature over a substantial length of the gauge section of the specimen and (ii) considerable and non-trivial efforts to open non-dominant cracks for post-mortem analysis. In the current study all FIB notches were located in one cross-sectional plane (t = 0.25"; W = 0.6") and evenly distributed on both faces of the specimen gauge (Figure 4).

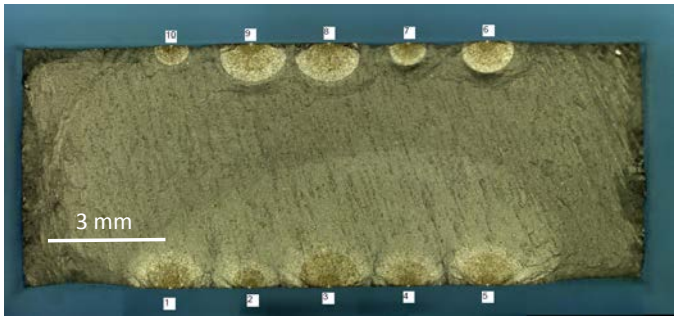

Figure 4. Fracture surface of SCT specimen with ten FIB notches

CRACK SIZE MEASUREMENT

Continuous crack size/shape evolution in CT specimens (W = 1.0"; t = 0.25") was measured by a direct current electric potential drop (DCEPD) technique as described in ASTM E647-11, section A1.5.3 and A6. The EPD wires were Alumel and had 0.015" in diameter. The current wires were also Alumel and had about 0.030" in diameter. All four of the wires were kept as short and as straight as possible. The method used in this study employs Johnson's equation to relate voltage measurements to crack length and the secant method of data reduction as described in ASTM E647-11, section X1.1. Since the tested material was relatively resistive, a reference voltage source was not used during testing because the required sensitivity and resolution for detecting crack change was available without it. The system used incorporates a practice of switching the current polarity during potential measurements to eliminate thermo-electric effects. A constant current of 3 amps was applied to a specimen. The system was capable to detect changes in crack length with a resolution of 0.0003".

The SCT specimens were periodically removed from the test frame and subjected to direct measurements/digital photography on a stationary optical microscope or scanning electron microscope (SEM) as the most accurate and reliable method. An instantaneous crack front location in both specimen types was made apparent by periodically heat tinting the specimen at various stopping points during the test.

TESTING AND RESULTS

All specimens were tested in laboratory air at 600F using servo-hydraulic MTS frames with FTA software. Triangular load wave-shape was applied with the frequency of 1 Hz.

Prior to testing several CT specimens were subjected to pre-cracking in compression at ambient conditions. Some basic information about the process parameters, applied to the two CT specimens discussed henceforth, is summarized in Table 2. Two values for pre-crack size are shown for each specimen as measured on both specimen sides.

Table 2. Compression pre-cracking parameters for CT specimens

Specimen	Min Stress, ksi	Max Stress, ksi	N, cycles	Pre-crack size, in
B1	-100	-5	289,929	0.0499/0.0491
C2	-60	-3	928,047	0.0238/0.0242

The SEM pictures (Figure 5) revealed an unusual concave shape and a featureless appearance of the compression pre-crack.

A purpose of testing the CT specimens was to compare the ASTM-recommended load-shedding procedure with the compression pre-cracking[1] as well as to evaluate the results as a potential common baseline for small-crack test results. Two test vendors were used to account for vendor-to-vendor scatter. Figure 6a compares the ASTM load shed results from two different vendors. A reasonable agreement between two datasets is observed with an apparent FCG threshold around 5.0 ksi*sqr (in) and a well defined transition from the near-threshold to the Paris region at about 10^{-7} in/cycle.

Slightly higher FCG rates, recorded by Vendor 2, can be attributed to some noticeable differences in the crack front curvature, different number of intermittent heat-tints used for the post-test analysis (compare A1 and A2 in Figure 7) or simply to an experimental scatter.

[1] The procedure is being currently evaluated for incorporation into the ASTM standard

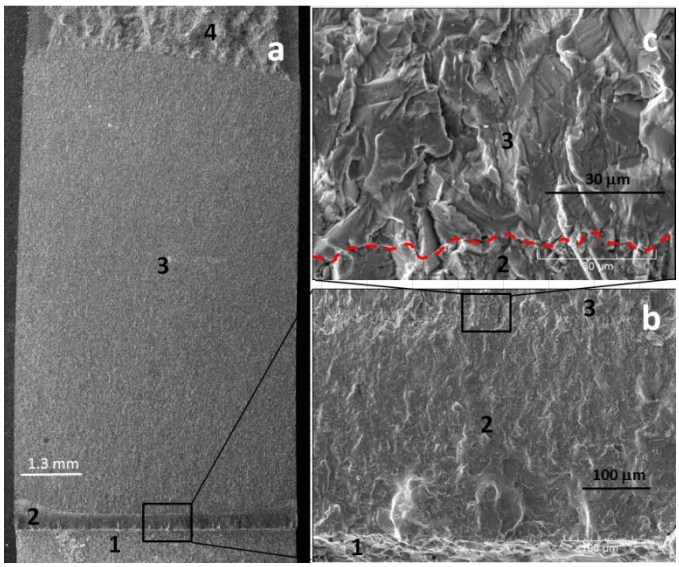

Figure 5. Overview (a) and microscopic details (b, c) of the compression pre-cracked CT specimen; 1- machined notch; 2- compression pre-crack; 3 – FCG growth under tension and 4 – final fracture

In case of the compression pre-cracked specimens, initial tensile loading was selected to provide a ΔK value slightly lower that the expected threshold stress intensity range of the tested material. If no crack propagation could be detected after a certain number[2] of loading cycles, the applied load was increased in small steps and fixed for the duration of the test after stable crack propagation was detected.

In case of specimen C2, this procedure resulted in the FCG behavior (Figure 6b) very similar to that registered under the ASTM load shedding test with an apparent FCG threshold around 5.0 ksi*sqr (in) and a well defined transition from the near-threshold to the Paris region at about 10^{-7} in/cycle.

The behavior of specimen B1 was quite different and warrants a closer consideration. As shown in Table 2, the pre-cracking of this specimen used high compressive stress of 100 ksi and was terminated after only 289,929 cycles when the crack growth rate decreased to less than 1.0×10^{-9} in/cycle. This was, apparently, not enough for the crack to reach a boundary of the compressive plastic zone associated with the notch. As the result of such premature termination of the pre-cracking process, there was some tensile residual stress left ahead of the crack tip. This may explain a "stable" crack propagation observed in this specimen under tensile loading with nominal ΔK values of about 4.5 ksi*sqr (in) which was well below the FCG threshold established by the ASTM load shed results from both vendors as well as by the C2 results generated after compression pre-cracking. As the crack continued to grow, it was getting less and less "help" from the tensile residual stress remaining in the specimen after the curtailed compression pre-cracking. This can explain the "paranormal" decrease in the FCG rate under nominally increasing ΔK values from 5.0 to 6.0 ksi*sqr (in) (see Figure 6b).

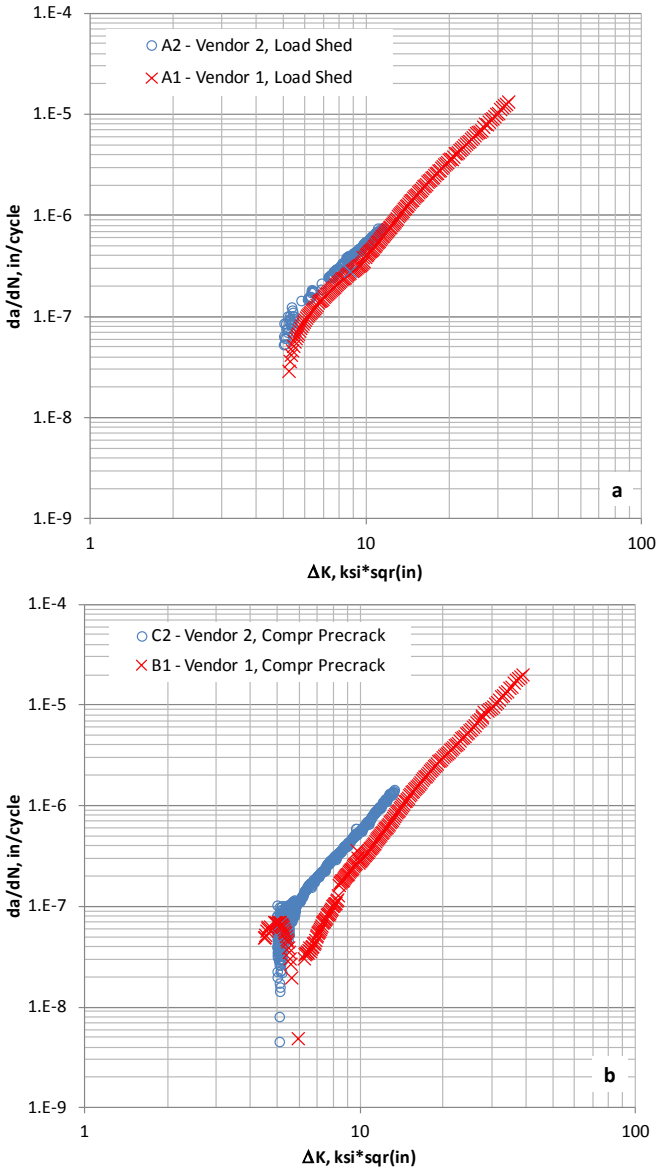

Figure 6. FCG curves for CT specimens tested by two different vendors at 600F and R=0.05 using ASTM load shedding (a) and compression pre-cracking (b) procedure

As can be seen from the Figure 7, a very slow crack propagation, immediately following the compression pre-cracking, resulted in noticeable fretting-corrosion of the

[2] Determined by dividing threshold FCG rate by the resolution of crack size measurement system used

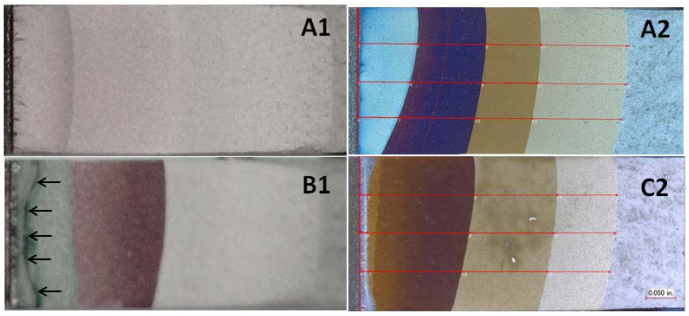

Figure 7. Fracture surfaces of CT specimens; FCG direction from left to right

fracture surface (black arrows), especially in the mid-thickness of the specimen, and, consequently, influenced the crack front shape and subsequent FCG behavior via well documented in literature oxide-induced crack closure [5]. It was concluded that the specimen B1 was pre-cracked incorrectly and the results were excluded from further consideration. A care was taken to extend compression pre-cracking of the following specimens until complete crack arrest.

Figure 8 compares all valid results obtained in this study on the CT geometry with the previous results [1] for the same material and test conditions, but generated using the SCT specimens with "large" cracks initiated from 0.02" (0.5 mm) long EDM notches. At high ΔK values both geometries produced similar results, however, as the ΔK values decrease, a trend towards slower crack growth rates in the SCT specimens becomes evident.

A purpose of testing the SCT specimens with FIB notches was to establish the smallest crack size that can be studied with this specimen geometry and then to evaluate the FCG behavior of given material in the presence of initial defects of that size.

Several specimens with multiple FIB notches ranging in surface length from 0.001" to 0.002" (0.025 mm to 0.05mm) were subjected to a constant-amplitude cyclic loading at 600F and R=0. The polished surfaces, immediately adjacent to the FIB notches, were periodically scrutinized in SEM or high-power optical microscope.

If no crack initiation was noticed after a predetermined number of cycles, the amplitude was increased and the entire procedure repeated. It has been established that FIB notches of surface length smaller than 0.002" (0.05 mm) were inefficient in initiating fatigue cracks in the given material, as several specimens failed from other locations whereas no damage could be observed in the vicinity of the notches.

Figure 9 shows the results for SCT specimen containing FIB notches of 0.002" (0.05mm) surface length located on both sides of the specimen. The pre-cracking and testing of the specimen was conducted at the nominal stress range of 130 ksi.

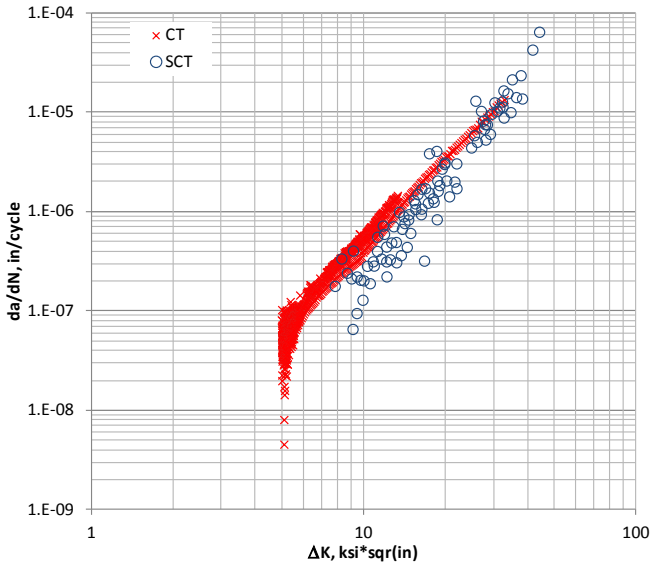

Figure 8. FCG results for large cracks generated using CT and SCT specimen geometry

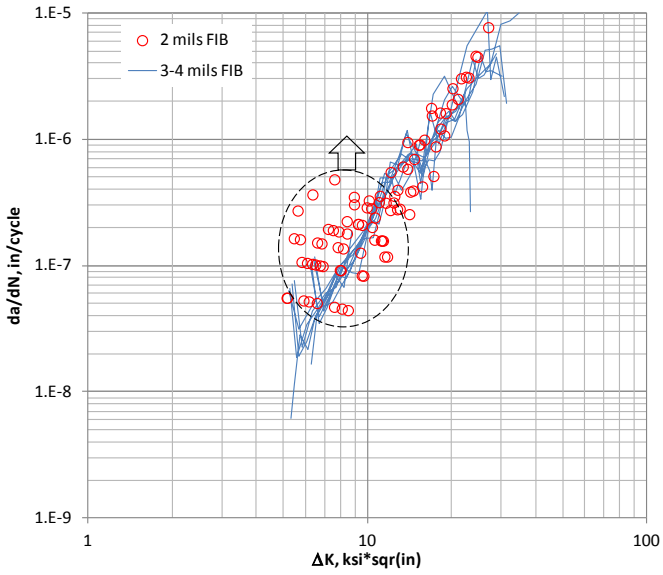

Figure 9. FCG results for small cracks generated using SCT specimen geometry with FIB notches

Note that in order to maintain clarity of the plot only results for two arbitrarily chosen cracks out of ten available in the specimen were plotted. The initial data points were taken at surface crack length 2c=0.0022" (0.0559 mm). When compared to the previous results from [1] for 0.003" and

0.004” long FIB notches, an obvious difference in the earlier crack propagation behavior can be seen.

Since previous study [1] had shown no significant difference between the cracks propagating from 0.076 mm-0.1 mm long FIB notches (identified as 3-4 mils FIB in Fig. 9) and much larger cracks propagating from typically used 0.5 mm long EDM notches, the difference seen in Figure 9 represents an extent of the small crack effect in the material studied. It follows that the effect is still present for cracks spanning several grain sizes, but disappears as soon as a crack surface length reaches 10 or more grain sizes.

DISCUSSION

Compressive cyclic loading was successfully used in [1] to pre-crack surface crack tension EDM-notched samples of a Ni-base alloy Inconel 718 and to generate fatigue crack growth data with minimal load history effects. Earlier, similarly encouraging results were produced on corner-crack geometry. The method definitely deserves further investigation and, potentially, a permanent place in the toolbox of practical approaches used to study the FCG in aero-GTE applications.

The current study adds to the on-going evaluation of the compression pre-cracking method by showing that it is capable of producing results similar to those obtained in accordance with the ASTM load shedding technique. At the same time, the results of Figure 6 and associated speculations clearly showed a potential risk of misusing the compression pre-cracking method by premature termination of the process that can adversely influence subsequent FCG behavior under tensile loading.

The risk appears to be especially high for the aero-GTE community that is used to a low-frequency loading during the FCG tests. It seems that incorporation of the compression pre-cracking will necessitate high-frequency loading capability so that the complete arrest of the compression pre-crack can be achieved in a reasonable amount of time, irrespective of the loading frequency of the subsequent (tensile) portion of the test.

The current experiments (Fig. 8) have shown different FCG behavior recorded at 600F with the CT and SCT specimens. Earlier studies at 1000F [6, 7], conducted on a similar, yet differently processed Inconel 718 material, did not reveal any specimen geometry effect under a low-frequency continuous cyclic loading. It is conceivable that this effect could be sensitive to the material microstructure (e.g., grain size) or simply masked by the environmental influences that had obviously reached a different degree at 600F and 1000F. However, the same earlier studies [6, 7] under *a different* loading - trapezoidal load-time path with a 5 min hold at the maximum - produced dissimilar results for the two specimen geometries that qualitatively agree with the outcome of the current study.

It had been suggested [7] that the variation in geometry between the two types of specimens may possibly allow for a different crack tip plastic strain during the peaks or the hold-time periods of a loading cycle. Therefore, relating damage to strain may explain the experimentally observed herein faster crack growth and reported in the literature lower fracture toughness in case of the CT geometry.

On the other hand, the nominal stress intensity factor by itself may not be sufficient to completely describe the elevated temperature crack propagation behavior in the aero-GTE hardware. For example, it is easy to see that the crack shape and dimension variations between the CT and SCT geometries would require substantially different background stresses in order to achieve the same value of the stress intensity factor.

As stated above, the majority of the FCG test results available in the literature was generated from the CT specimens that, unfortunately, are not suitable to study small cracks. By necessity, at least some comparisons reported in the literature between so-called “large” and “small” cracks may include hidden specimen geometry component. While for certain material/test conditions combination this specimen geometry effect may be negligible, the current study and the available literature data clearly showed that for the aero-GTE applications it needs to be properly accounted for.

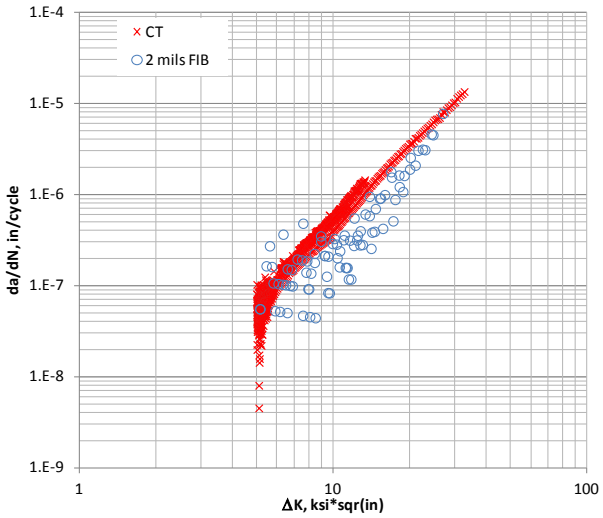

Figure 10. FCG results for small cracks generated using SCT specimen geometry with 2-mill FIB notches and large cracks generated using CT specimen geometry

For example, Figure 9 without a doubt shows the small-crack effect – up to an order of magnitude acceleration in the

initial propagation rate between cracks growing from the 2-mil FIB notches as compared to the larger cracks in *the same* SCT geometry. However, a similar comparison between these data points and the CT data for the same material and test conditions would have erroneously shown an absence of the small-crack effect (Figure 10), since large cracks propagating in the CT specimens almost always grow faster than the small cracks initiated from the 2 mils long FIB notches in the SCT specimen. Obviously, in this case a real small-crack effect is hidden behind the specimen geometry effect similar to that depicted in Figure 8.

SUMMARY AND CONCLUSIONS

Large cracks in DP718 material were studied at 600F using the ASTM E647 prescribed load-shedding and compression pre-cracking methodology on widely used compact tension specimen geometry.

After correct application of compression pre-cracking both approaches had shown a reasonably consistent behavior with the FCG threshold around 5.0 ksi*sqr (in) and well defined "knee" around 10^{-7} in/cycle separating the near-threshold crack growth from the Paris regime. In particular, comparison of the two tests conducted by the same vendor (A2 and C2 in Figure 6) revealed no significant difference between the ASTM load shed results and the results generated after compression pre-cracking.

On the other hand, premature termination of the compression pre-cracking process substantially altered the subsequent FCG behavior under tensile loading via residual tensile stresses and oxide-induced crack closure. Adoption of the compression pre-cracking method by the aero-GTE community will necessitate high-frequency loading capability even for the low-frequency FCG tests.

The FCG results generated in this study on the CT geometry were compared with the previous results for the SCT specimens with large cracks initiated from 0.02" long EDM notches. At high ΔK values both geometries produced similar results, however, as the ΔK values decreased, a trend towards slower FCG rates in the SCT specimens became evident.

Small cracks in the current study had an optimized (semi-elliptical rather than square) shape and were of the smallest dimensions that could be tested in the given SCT geometry.

Comparison of cracks initiated from 0.002" long FIB notches to the previous results [1] for 0.003" and 0.004" long FIB notches has revealed up to ten times acceleration in the initial propagation rates at the same ΔK values. The dimensional extent of this small-crack effect is consistent with the microstructural condition of the tested material (average grain diameter of 0.0003" or 0.008 mm) and prevailing empirical evidence showing that for a majority of polycrystalline metallic materials *microstructurally* small crack behavior occurs within initial 5 to 10 grain sizes.

ACKNOWLEDGMENTS

Mr. J. T. Hartman and Mr. B. Gregory of Honeywell Materials Laboratory assisted with the FCG specimens preparation and testing. The results were generated as part of the Probabilistic Design for Rotor Integrity (PDRI) program and the subsequent Probabilistic Integrity and Risk Assessment of Turbine Engines (PIRATE) program managed by Dr. R. Craig McClung of Southwest Research Institute (SwRI) who actively participated in valuable technical discussions of the generated results and their analysis. The funding was provided by the Federal Aviation Administration (Grants 05-G-005 and 11-G-009) through subcontracts from SwRI.

REFERENCES

1. Lenets Y. N. Practical aspects of fatigue crack growth in aero-GTE applications. GT2012-68736, Proceedings of the ASME TURBO EXPO 2012, Copenhagen, Denmark.
2. Suresh S. Crack initiation in cyclic compression and its application. Engineering Fracture Mechanics, 1985, Volume 21, Number 3, pp. 452-463.
3. Pippan R. The growth of short cracks under cyclic compression. Fatigue & Fracture of Engineering Materials & Structures, 1987, Volume 9, Issue 5, pp. 319-328.
4. Forth S. C., Newman Jr. J. C. and Forman R. G. On generating fatigue crack growth thresholds. Int J Fatigue 2003, 25, pp. 9–15.
5. Romaniv O. N., Tkach A. N. and Lenets Yu N. Effect of fatigue crack closure on near-threshold crack resistance of structural steels. Fatigue & Fracture of Engineering Materials & Structures, 1987, Volume 10, Issue 3, pp. 203–212.
6. Popp H. G., Coles A. Subcritical crack growth criteria for Inconel 718 at elevated temperature. Proc. Air Force Conf. on Fatigue and Fracture of Aircraft Structures and Materials, Wright-Petterson A. F. Base, Dayton, OH, 1970, p. 71-86.
7. Coles A., Johnson R. E., Popp H. G. Utility of surface-flawed tensile bars in cyclic life studies. J. Egngn Mater and Techn., 1976, p. 305-315.